A Global Model for the Identification of the Dominant Reactions for Atomic Oxygen in He/O_2 Atmospheric-Pressure Plasmas

Gan Young Park, Yong Jun Hong, Hyun Woo Lee, Jae Yoon Sim, Jae Koo Lee*

Atmospheric pressure plasmas have attracted great interests and been widely used in biomedical applications such as sterilization, coagulation, wound healing, and cancer cells treatment. The reactive oxygen species (ROS) generated in atmospheric pressure plasmas have been believed to play a crucial role in these biomedical applications. The experimental measurement of the atomic oxygen density showed that the highest density was measured at an admixture of 0.5% of O_2. The similar trend of the atomic oxygen density varying the concentration of O_2 was reproduced through a global model of He/O_2 in atmospheric pressure plasmas. The evolution of the dominant production and loss reactions for the atomic oxygen was analyzed. With increase in the concentration of O_2, the atomic oxygen was produced mainly by the dissociation of O_2 and lost through the recombinations with themselves and oxygen molecules.

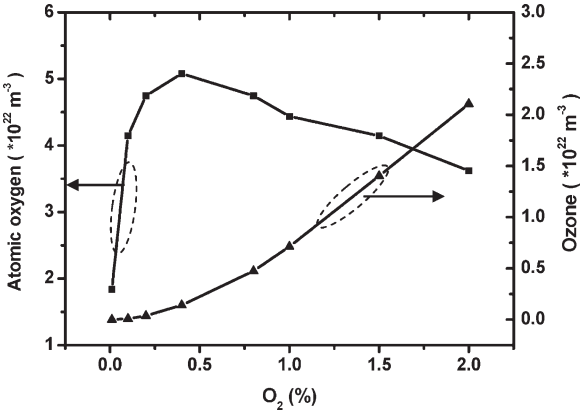

Introduction

Atmospheric pressure plasmas have been widely used in biomedical applications such as sterilization,[1] coagulation,[2] wound healing,[3] and inducing apoptosis of cancer cells[4] due to their great reactivity, low temperature property, and no needs for the expensive and complex vacuum system. Various kinds of atmospheric pressure plasmas such as the atmospheric pressure plasma jet, the dielectric barrier discharges, and the needle plasma have been developed and their generation has been achieved over a wide spectrum from dc, through kilohertz and megahertz to microwave.[5–8] However, a quantitative diagnostic of atmospheric pressure plasmas is quite challenging due to their often small dimension, short duration, and the limited applicability of conventional low pressure diagnostic techniques. As a result, a computer simulation is a powerful tool that can complement experimental observations and help in unraveling the physics underpinning these discharges.

Admixtures of He and O_2 are often used in atmospheric pressure plasmas because of their satisfactory compromise between plasma stability and chemical reactivity.[9,10] The reactive oxygen species (ROS) are believed to play a crucial role in these biomedical applications.[1,9] The chemistry of these discharges is therefore of great interest and understanding the main reactions involved in the generation of reactive species is a first step needed in order

J. K. Lee, G. Y. Park, H. W. Lee, J. Y. Sim
Department of Electronic and Electrical Engineering, Pohang University of Science and Technology, Pohang 790-784, S. Korea
Fax: (+82) 54 279 2903; E-mail: jkl@postech.ac.kr
Y. J. Hong
Department of Physics, Pohang University of Science and Technology, Pohang 790-784, S. Korea

DOI: 10.1002/ppap.200900084

to optimize the plasmas. To that end, we have developed a global model[11,12] for He/O_2 discharges. The model incorporates a total of 98 reactions, something that cannot be handled by today's particle-in-cell Monte Carlo collision simulations and that slows down significantly fluid models. Although this model is not able to capture spatial variations often observed in actual discharges, it is a powerful tool for identifying main species and reactions from a large set of chemical processes.

Model

The global model was widely adopted as a tool to understand the characteristics of the low-pressure capacitively-coupled discharges,[11,13] the hollow cathode,[14] and the atmospheric pressure glow discharge.[12] Its fast computational time and the capability of the easy implementation for taking into account a number of species and reactions are the great advantages of this model to be chosen.

In the model of He/O_2 atmospheric pressure plasmas, 15 species, namely, electrons *e*, helium ions He^+, excited helium atoms He^*, dimer helium ions He_2^+, excited dimer He_2^*, positive oxygen molecule ions O_2^+, negative oxygen molecule ions O_2^- and O_3^-, excited oxygen molecules $O_2(^1\Delta_g)$ and $O_2(^1\Sigma_g^+)$, ozone O_3, ground-state atomic oxygen $O(^3P)$, positive atomic oxygen ions O^+, negative atomic oxygen ions O^-, excited oxygen atoms $O(^1D)$ are considered. Our model of He/O_2 includes 98 reactions for He/O_2 mixture selected from publications on discharge modeling in the literatures.[11,15–23]

The model describes a plasma source of volume V and its surface area S. The plasma is assumed to be nearly spatially uniform and the power is absorbed uniformly into the plasma. In an arbitrary volume (V) enclosed by the surface area (S), the time-dependent particle balance equations for each species density (n_k) are taken to be

$$\frac{d}{dt}(n_k) = (s_k - l_k) - \left(\frac{S}{V}\right)\Gamma_k \tag{1}$$

that describes the balance between source and loss to result from the reactions among species and the wall loss due to the thermal diffusion, where n_k is the density of species, s_k and l_k are the generation and loss rate due to the chemical reactions, respectively, and Γ_k is the flux into the boundary. Assuming the ions and radicals are Maxwellian distributions with the room temperature, the flux at the boundary is defined as

$$\Gamma_k = \frac{1}{4} n_k \overline{v}_k \tag{2}$$

where $\overline{v}_k$ is the averaged velocity of species. For the quasi-neutrality, the flux into the boundary of the electrons is defined as

$$\Gamma_e = \sum_i \Gamma_{+,i} - \sum_j \Gamma_{-j} \tag{3}$$

where $\Gamma_\pm$ is a positive or negative ion flux at the boundary.

The power balance equation to consider the balance between the input absorption power and the power loss of electrons by the collisions with other species is taken to be

$$\frac{d}{dt}\left(\frac{3}{2} n_e T_e\right) = P_{abs} - P_e \tag{4}$$

where T_e is the electron temperature in eV, P_{abs} the input power density, and P_e is the power loss of electrons due to the chemical reactions. Electrons are assumed to have a Maxwellian energy distribution function. Equation (1) for each species and Equation (4) were solved simultaneously to calculate the each species density and the electron

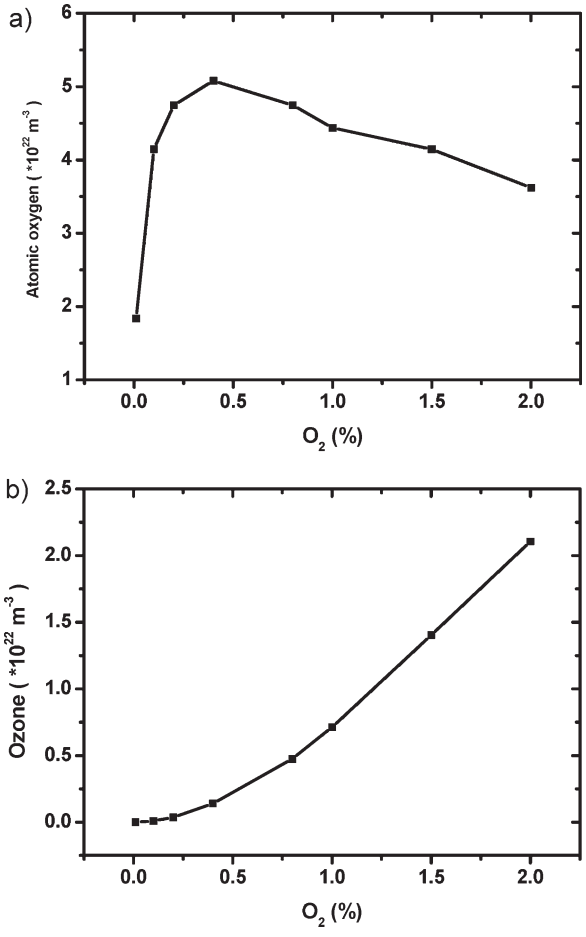

Figure 1. (a) The atomic oxygen and (b) the ozone density for various concentration of O_2 (absorbed power = 330 W · cm^{-3}).

DOI: 10.1002/ppap.200900084

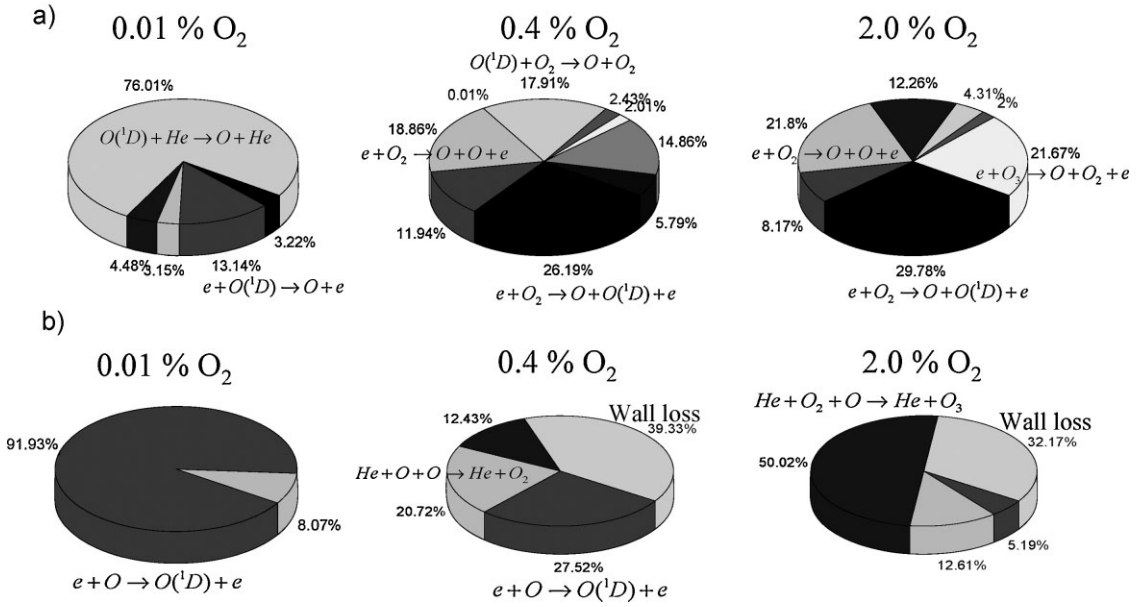

Figure 2. Diagrams for proportions of the atomic oxygen (a) production and (b) loss reactions concentrations of O_2, 0.01, 0.4, and 2.0%.

temperature. The densities of neutral species of helium and oxygen molecules were fixed at the initial values given by the fraction of an admixture at the atmospheric pressure. The gas temperature was fixed at room temperature, 300 K since the atmospheric pressure plasmas for biomedical applications are non-thermal discharges and their gas temperature is not far from the room temperature. For the simplicity, the gas heating due to the collisions among feeding gases and other species was not considered.

Results and Discussion

Figure 1(a) and (b) show the atomic oxygen and ozone densities in He/O_2 atmospheric pressure discharges while varying the concentration of O_2 with the input power of 330 $W \cdot cm^{-3}$, which is the power absorbed when the input power of 10 W applied to the plasma volume of 30 mm^3 and is close to the magnitude used in ref.[6] It is believed that those species are crucial agents to deactivate bacteria and cause disinfections or sterilizations.[1,9] Knake et al.[6] measured the atomic oxygen density in the discharge core while changing the concentration of O_2 and showed the highest oxygen production at an admixture of 0.5% of O_2. As shown in Figure 1(a), the similar trend is observed through the global model and the maximum atomic oxygen production appears at 0.4% of O_2. However, the ozone density does not show a maximum value at a certain admixture of O_2 up to 2.0% and keeps growing with increase in the concentration of O_2.

The evolution of the atomic oxygen density with the concentration of O_2 is analyzed in terms of the dominant production and loss reactions for the atomic oxygen. The diagrams in Figure 2(a) and (b) show the proportion of each production and loss reaction rate for the atomic oxygen with respect to the total reaction rates. At the low concentration of O_2 (0.01%), most of atomic oxygen are generated through the de-excitation processes of $O(^1D)$ by colliding with electrons and neutral helium atoms, as shown in Figure 2(a). With increase in the concentration to 0.4% of O_2, the atomic oxygen is produced through the dissociation processes of oxygen molecules by electrons and partly, the de-excitation of $O(^1D)$ by collisions with oxygen molecules. At the high concentration of O_2, the dissociations of O_2 and O_3 are the dominant processes to produce the atomic oxygen. Figure 2(b) shows the proportion of the dominant loss reactions for the atomic oxygen. At the low concentration (0.01%) of O_2, the atomic oxygen more than 90% are lost through the excitation process to $O(^1D)$ by collisions with electrons. At the concentration of O_2 where the atomic oxygen density is maximum (0.4%), the portion of the excitation process of the atomic oxygen to $O(^1D)$ is reduced and the thermal wall losses are the most dominant process and the recombination between the atomic oxygens is significant. At the high concentration of O_2 (2.0%), the recombination of the atomic oxygen and oxygen molecules by three body collisions with helium atoms are the most dominant loss process for the atomic

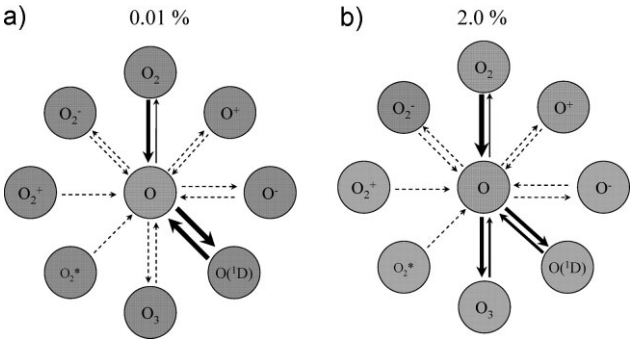

Figure 3. Diagrams for the relation between the atomic oxygen and other oxygen species for 0.01 and 2.0% of O_2.

oxygen, and since those recombination processes produce the ozone, its density grows with increase in the concentration of O_2.

Figure 3 shows the relations of the atomic oxygen with other oxygen species such as the excited oxygen and ionized oxygen molecules, and the width of the arrows indicates the relative magnitude of the reaction rate. At the low concentration of O_2 (0.01%), the atomic oxygen is excited by electrons into $O(^1D)$ and the $O(^1D)$ is de-excited into the ground state oxygen colliding with the electrons and oxygen molecules. At the high concentration of O_2 (2.0%), the atomic oxygen is generated by the dissociation of oxygen molecules rather than the de-excitation of $O(^1D)$ and is lost by the recombination with the oxygen molecules producing the ozone.

In the steady state, the total production and loss rates for a species have to be equal and its density remains constant as a result of a balance between them. Figure 4(a) shows the sum of all production (or loss) reaction rates for the atomic oxygen. Although the atomic oxygen density increases with increase in the concentration of O_2 to 0.4%, the total reaction rate is reduced. This results from the decrease in the electron density while increasing the concentration of O_2 since the oxygen molecule is the electro-negative gas. Figure 4(b) shows the total rates of reactions to produce the atomic oxygen through the dissociation of oxygen molecules and its proportion to total production rate. While the concentration of O_2 increases, the dissociation of oxygen molecules increases and the dissociation processes become significant to produce the atomic oxygen. The atomic oxygen can be lost through the electron-dominated loss reactions such as excitation, ionization, and attachment to change the atomic oxygen to $O(^1D)$, O^+, and O^-. Figure 4(c) compares the proportions of the electron-dominated loss reactions rate and the dissociative productions rate to total reaction rate. It is noted that the reduction rate of the electron-dominated losses is larger than the increase rate of the dissociative productions with increase in the concentration of O_2 to 0.4%. Therefore, it is likely that the increase

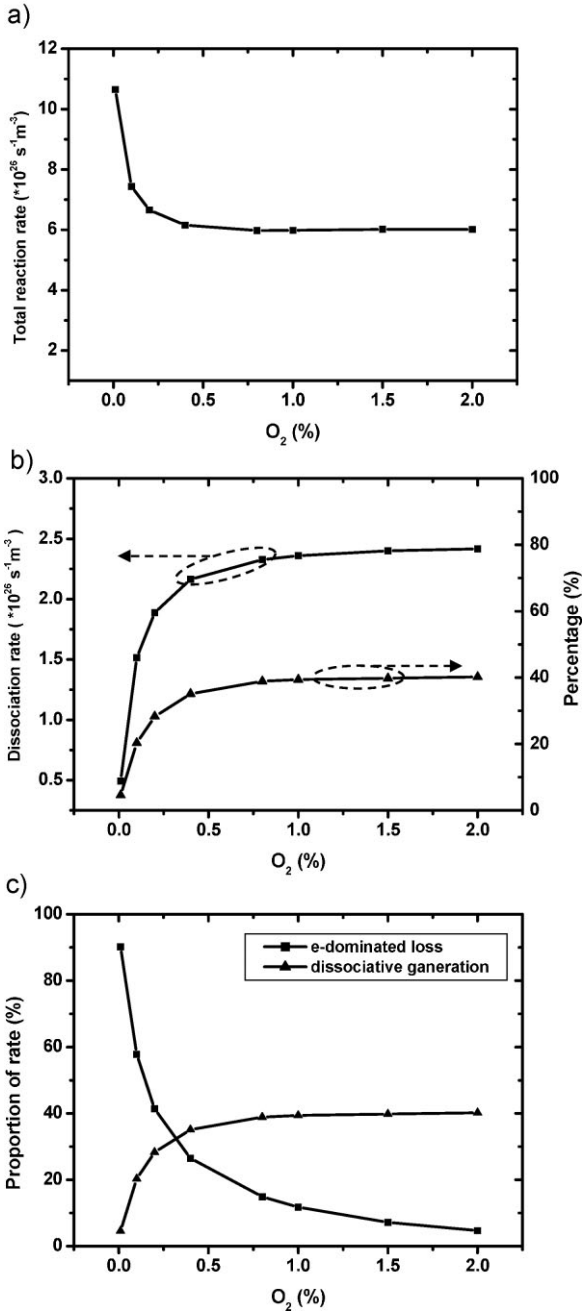

Figure 4. (a) The total reaction rate and (b) the dissociative production rate for the atomic oxygen and its proportion with respect to total production rate and (c) the comparison of the proportions of the electron-dominated loss and the dissociative generation for the atomic oxygen for various admixtures of O_2.

in the atomic oxygen density at the low concentrations of O_2 (<0.4%) is attributed to the decrease in the electron-dominated loss reactions rate rather than the increase in the dissociative productions.

Figure 5 shows the evolution of the proportions of the dominant groups of the atomic oxygen loss processes such

DOI: 10.1002/ppap.200900084

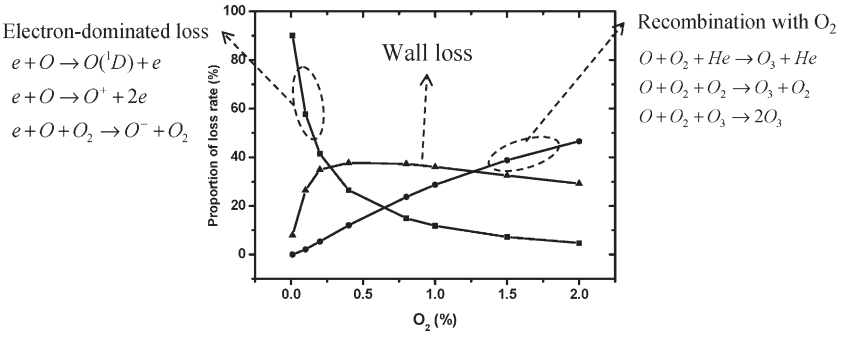

Figure 5. The loss rates of the electron-dominated loss, the wall loss, and the recombinations loss with O_2 concentrations of O_2.

as the electron-dominated losses, thermal wall loss, and recombination losses with oxygen molecules while varying the concentration of O_2. At the low concentration of O_2 less than 0.3%, the electron-dominated loss reactions are the most dominant in the loss groups and are reduced with increase in the admixture of O_2 due to the decrease in the electron density. At the intermediate concentration (<1.0%), the wall loss dominates because the wall loss is proportional to the density and the atomic oxygen density increases with increase in the concentration of O_2, as shown in Figure 1(a). At the high concentration of O_2 (>1.0%), since the population of oxygen molecules increases, the recombinations of the atomic oxygen with oxygen molecules are the most dominant processes and the ozone is produced as a byproduct. This evolution of the dominant loss reactions seems to be closely related with the density profile of the atomic oxygen as varying the concentration of O_2.

Figure 6 shows the atomic oxygen densities for different input powers while varying the concentration of O_2 and they are normalized by a maximum value for each case to compare each other. With decrease in the input power, the concentration of O_2 to show a maximum density moves to lower value. The reduction of the relative atomic oxygen density with increase in the admixture of O_2 is faster at the case of the lower input power, as shown in Figure 6. The evolution of the dominant loss processes for the atomic oxygen is analyzed with change in the input power. With increase in the power absorbed at the admixture of 0.4% O_2, the proportion of the recombinations with oxygen molecules and the wall loss are reduced and the electron-dominated losses are increased, as shown in Figure 7(a). For the case of 0.05% of O_2, the transition of the dominant loss process from the wall loss to the electron-dominated loss is observed while increasing the input power, as shown in Figure 7(b).

The global model is able to consider lots of reactions due to its fast computation time. If the model can select the

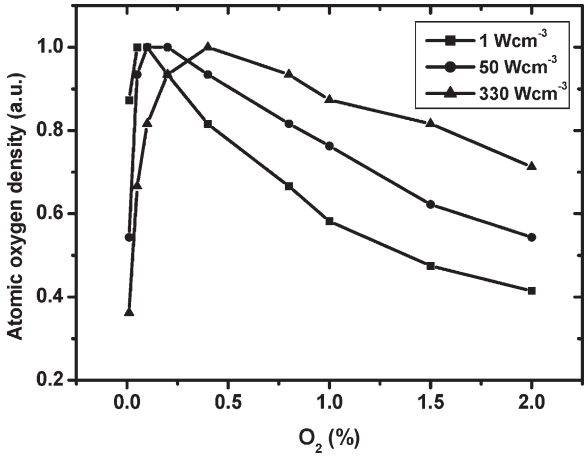

Figure 6. The atomic oxygen density normalized by the maximum density for different input power of 1, 50, and 330 $W \cdot cm^{-3}$ concentrations of O_2.

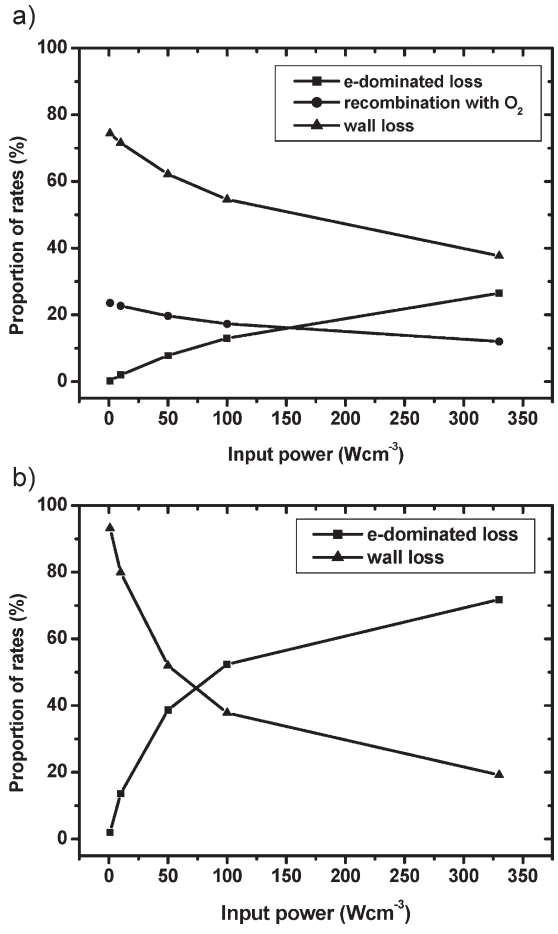

Figure 7. The proportions of different groups of loss processes for the atomic oxygen at (a) 0.4% and (b) 0.05% of O_2.

Table 1. A list of key reactions for He/O_2 mixture. (T_e in volts and T in kelvins.)

No.	Reaction	Rate constant	No.	Reaction	Rate constant
		$cm^3 \cdot s^{-1}$			$cm^3 \cdot s^{-1}$
R1[a)]	$O_2^+ + e \rightarrow 2O$	4.8E-7	R19[f)]	$He^* + O_2 \rightarrow He + O_2^+ + e$	2.4E-10
R2[a)]	$e + O_2 \rightarrow O^- + O$	8.8E-11 $\exp(-4.4/T_e)$	R20[g)k)]	$He + O_2 + O \rightarrow He + O_3$	6.27E-34
R3[a)]	$e + O_2 \rightarrow O_2^+ + 2e$	9.0E-10T_e $\exp(-12.6/T_e)$	R21[h)]	$e + He \rightarrow He^* + e$	2.3E-10$T_e^{0.31}$ $\exp(-19.8/T_e)$
R4[a)]	$O^- + O \rightarrow O_2 + e$	2.0E-10	R22[h)]	$e + He \rightarrow He^+ + 2e$	2.5E-12$T_e^{0.68}$ $\exp(-24.6/T_e)$
R5[b)]	$O_2 + O^+ \rightarrow O_2^+ + O$	2.0E-11	R23[h)]	$e + He_2^+ \rightarrow He^* + He$	5.386E-7$T_e^{0.5}$
R6[a)]	$e + O_2 \rightarrow O_2(^1\Delta_g) + e$	1.7E-9 $\exp(-3.1/T_e)$	R24[h)k)]	$He^* + 2He \rightarrow He_2^* + He$	1.3E-33
R7[a)]	$O^- + O_2(^1\Delta_g) \rightarrow O_3 + e$	3.0E-10	R25[h)k)]	$He^+ + 2He \rightarrow He_2^+ + He$	1.3E-31
R8[a)]	$O^- + O_2(^1\Delta_g) \rightarrow O_2^- + O$	1.0E-10	R26[j)]	$He_2^* + He_2^* \rightarrow He_2^+ + 2He + e$	1.5e-9
R9[a)]	$e + O_2 \rightarrow O + O(^1D) + e$	5.0E-8 $\exp(-8.4/T_e)$	R27[i)]	$O(^1D) + O_2 \rightarrow O + O_2$	3.0e-11
R10[a)]	$e + O \rightarrow O(^1D) + e$	4.2E-9 $\exp(-2.25/T_e)$	R28[d)]	$O(^1D) + He \rightarrow O + He$	1.0e-13
R11[c)]	$O_2(^1\Sigma_g^+) + O_3 \rightarrow O + 2O_2$	1.5E-11	R29[e)]	$O_2(^1\Sigma_g^+) + O \rightarrow O_2(^1\Delta_g) + O$	3.0e-12
R12[a)]	$O^* + O_2 \rightarrow O + O_2(^1\Sigma_g^+)$	2.0E-11	R30[i)]	$e + O_3 \rightarrow O^- + O_2$	9.3E-10$T_e^{-0.62}$
R13[d)]	$e + O_2 \rightarrow O + O + e$	4.2E-9 $\exp(-5.6/T_e)$	R31[i)]	$e + O_3 \rightarrow O + O_2^-$	2.0e-10
R14[e)]	$O_2(^1\Delta_g) + O_3 \rightarrow 2O_2 + O^*$	1.0E-11	R32[i)]	$O_3^- + O_2^+ \rightarrow 2O + O_3$	1.01E-7(300/T)$^{0.5}$
R15[d)]	$e + O \rightarrow O^+ + 2e$	9.0E-9$T_E^{0.7}$ $\exp(-13.6/T_e)$	R33[i)]	$e + O_3 \rightarrow O + O_2 + e$	1E-8(300/T)$^{0.5}$
R16[e)]	$O^- + O_3 \rightarrow O_3^- + O$	5.3E-10	R34[d)]	$He^+ + O_2 \rightarrow O^+ + O + He$	1.07E-9(T/300)$^{0.5}$
R17[e)]	$O_3^- + O \rightarrow 2O_2 + e$	3.0E-10	R35[e)]	$O_2^- + M \rightarrow O_2 + M + e$	2.7E-10(T/300)$^{0.5}$ $\exp(-5\,590/T)$
R18[e)]	$O_3^- + O \rightarrow O_2^- + O_2$	3.2E-10			

[a)]Ref. [11]; [b)]Ref. [15]; [c)]Ref. [16]; [d)]Ref. [17]; [e)]Ref. [18]; [f)]Ref. [19]; [g)]Ref. [20]; [h)]Ref. [21]; [i)]Ref. [22]; [j)]Ref. [23]; [k)]Rate constants are in $cm^6 \cdot s^{-1}$.

dominant reactions of those typically chosen in other models such as fluid and particle-in-cell models, it would help them to reduce their computation time. For He/O_2 mixture, 35 key reactions of 98 reactions used in our model are selected by means of analyzing the reaction rates for each species and picking up the dominant reactions, as listed in Table 1. Figure 8 shows the comparisons of the electron and the atomic oxygen density obtained from calculations with all 98 reactions and selected 35 reactions. The model with the selected 35 key reactions can reproduce the quite close results for electron and atomic oxygen densities to those obtained from the model with 98 reactions for wide ranges of the input power, as shown in Figure 8(a) and (b).

Conclusion

We have developed a global model of He/O_2 atmospheric pressure discharges widely used in the biomedical applications such as sterilization, coagulation, and wound healing to identify the dominant reactions and the main species. Similar trend to an experimental measurement of the atomic oxygen density was observed through the global

DOI: 10.1002/ppap.200900084

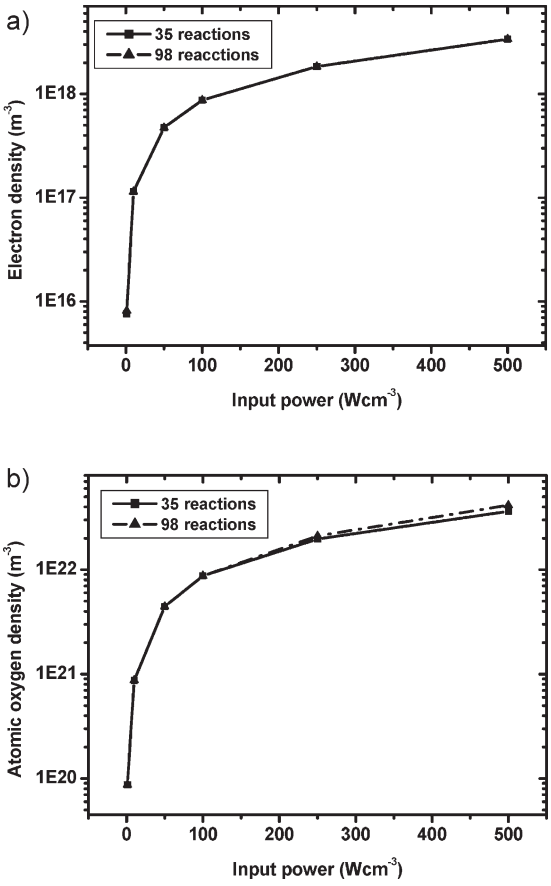

Figure 8. The comparisons of (a) the electron density and (b) the atomic oxygen density obtained from models to consider 35 key reactions and 98 reactions.

model while varying the concentration of O_2. The maximum atomic oxygen density appeared at an admixture of 0.4% of O_2 when the input power was 330 $W \cdot cm^{-3}$. With increase in the concentration of O_2, the dissociation of O_2 increased to produce the atomic oxygen, and the recombinations of the atomic oxygen with themselves or oxygen molecules and the thermal wall loss became the dominant loss processes for the atomic oxygen. With decrease in the input power, the maximum density of the atomic oxygen was observed at lower concentration of O_2. The 35 key reactions of He/O_2 were selected through the analysis of reaction rates for each species and they reproduced almost same results as those obtained from the calculations to take into account 98 reactions. The global model could be used to identify the dominant reactions and would be helpful to reduce the computational time for simulations of biomedical atmospheric pressure discharges.

Acknowledgements: The authors are grateful to Dr. *F. Iza* in Loughborough University, UK for his comments helpful to develop the model. This work was supported by the *Korea Science and Engineering Foundation* (KOSEF) grant funded by the *Korea government* (MOST) (No. R01-2007-000-10730-0) and the *Brain Korea 21 Project* in 2009.

Received: June 1, 2009; Revised: December 8, 2009; Accepted: December 30, 2009; DOI: 10.1002/ppap.200900084

Keywords: atmospheric pressure plasma; atomic oxygen; computer modeling; global model; reactive oxygen species (ROS)

[1] M. Laroussi, *Plasma Process. Polym.* **2005**, *2*, 391.
[2] S. U. Kalghatgi, G. Fridman, M. Cooper, G. Nagaraj, M. Peddinghaus, M. Balasubramanian, V. N. Vasilets, A. F. Gutsol, A. Fridman, G. Friedman, *IEEE Trans. Plasma Sci.* **2007**, *35*, 1559.
[3] G. Fridman, G. Friedman, A. Gutsol, A. B. Shekhter, V. N. Vasilets, A. Fridman, *Plasma Process. Polym.* **2008**, *5*, 503.
[4] G. C. Kim, G. J. Kim, S. R. Park, S. M. Jeon, H. J. Seo, F. Iza, J. K. Lee, *J. Phys. D: Appl. Phys.* **2009**, *42*, 032005; *Europhys. News* **2009**, *40*, 14.
[5] M. Moravej, X. Yang, R. F. Hicks, J. Penelon, S. E. Babayan, *J. Appl. Phys.* **2006**, *99*, 093305.
[6] N. Knake, K. Niemi, S. Reuter, V. S. Gathen, J. Winter, *Appl. Phys. Lett.* **2008**, *93*, 131503.
[7] E. Stoffels, I. E. Kieft, R. E. J. Sladek, *J. Phys. D: Appl. Phys.* **2003**, *36*, 2908.
[8] J. Choi, F. Iza, H. J. Do, J. K. Lee, M. H. Cho, *Plasma Sources Sci. Technol.* **2009**, *18*, 025029.
[9] X. Deng, J. Shi, M. G. Kong, *IEEE Trans. Plasma Sci.* **2006**, *34*, 1310.
[10] S. J. Kim, T. H. Chung, S. H. Bae, S. H. Leem, *Appl. Phys. Lett.* **2009**, *94*, 141502.
[11] M. A. Lieberman, A. J. Lichtenberg, *Principle of Plasma Discharges and Materials Processing*, Wiley, New York 2005.
[12] G. Y. Park, H. W. Lee, G. C. Kim, J. K. Lee, *Plasma Process. Polym.* **2008**, *5*, 569.
[13] S. J. Kim, M. A. Lieberman, A. J. Lichtenberg, J. T. Gudmundsson, *J. Vac. Sci. Technol., A* **2006**, *24*, 2025.
[14] H. J. Lee, J. K. Lee, *Jpn. J. Appl. Phys.* **1996**, *35*, 6252.
[15] A. B. Rakshit, H. M. P. Stock, D. P. Wareing, N. D. Twiddy, *J. Phys. B: At. Mol. Phys.* **1978**, *11*, 4237.
[16] D. L. Baulch, R. A. Cox, P. J. Crutzen, R. F. Hampson, Jr., J. A. Kerr, J. Troe, R. T. Watson, *J. Phys. Chem. Ref. Data* **1982**, *11*, 327.
[17] D. S. Stafford, M. J. Kushner, *J. Appl. Phys.* **2004**, *96*, 2451.
[18] C. Soria, F. Pontiga, A. Castellanos, *Plasma Sources Sci. Technol.* **2004**, *13*, 95.
[19] W. Lindinger, A. L. schmeltekopf, F. C. Fehsenfeld, *J. Chem. Phys.* **1974**, *61*, 2890.
[20] J. Y. Jeong, J. Park, I. Henins, S. E. Babayan, V. J. Tu, G. S. Selwyn, G. Ding, R. F. Hicks, *J. Phys. Chem. A* **2000**, *104*, 8027.
[21] S. Rauf, M. J. Kushner, *J. Appl. Phys.* **1999**, *85*, 3460.
[22] J. T. Gudmundsson, I. G. Kouznetsov, K. K. Patel, M. A. Lieberman, *J. Phys. D: Appl. Phys.* **2001**, *34*, 1100.
[23] R. Deloche, P. Monchicourt, M. Cheret, F. Lambert, *Phys. Rev. A* **1976**, *13*, 1140.